

Correlated Electronic Structures and the Phase Diagram of Hydrocarbon-based Superconductors

Minjae Kim¹, Hong Chul Choi², Ji Hoon Shim^{2,1,*} and B. I. Min^{1†}

¹*Department of Physics, PCTP, Pohang University of Science and Technology, Pohang, 790-784, Korea and*

²*Department of Chemistry, Pohang University of Science and Technology, Pohang, 790-784, Korea*

(Dated: September 24, 2018)

We have investigated correlated electronic structures and the phase diagram of electron-doped hydrocarbon molecular solids, based on the dynamical mean-field theory. We have found that the ground state of hydrocarbon-based superconductors such as electron-doped picene and coronene is a multi-band Fermi liquid, while that of non-superconducting electron-doped pentacene is a single-band Fermi liquid in the proximity of the metal-insulator transition. The size of the molecular orbital energy level splitting plays a key role in producing the superconductivity of electron-doped hydrocarbon solids. The multi-band nature of hydrocarbon solids would boost the superconductivity through the enhanced density of states at the Fermi level.

PACS numbers: 71.27.+a, 74.70.Kn, 74.70.Wz, 74.20.Pq

Since the discovery of high T_C superconductors, the role of the electronic correlation in the superconductivity has been a subject of intensive investigation. While conventional BCS superconductors such as Nb and MgB₂ have good metallic nature of Fermi liquid,[1, 2] unconventional superconductors such as doped cuprate and iron pnictide show bad metallic behavior due to their strong electronic correlation.[3, 4] The correlation issue exists in carbon-based π -electron superconductors too. Ca-doped graphite (CaC₆) shows conventional superconductivity with weak electronic correlation,[5] whereas Cs₃C₆₀ exhibits unconventional superconductivity with strong electronic correlation.[6]

New π -electron superconductors have been recently discovered in polycyclic aromatic hydrocarbon (PAH)-based molecular solids: K₃picene ($T_c=18$ K), K₃coronene ($T_c=15$ K), K₃phenanthrene ($T_c=5$ K), and K₃1,2;8,9-dibenzopentacene ($T_c=33$ K).[7–10] These superconductors were also reported to have strong correlation.[11–14] On the other hand, a similar PAH-based molecular solid, K-doped pentacene, does not have superconductivity, but exhibits only the metal-insulator transition (MIT) behavior.[15] Note that both picene and pentacene are composed of five benzene rings with slightly different arrangements, as shown in Fig. 1. The different ground states in K-doped picene and K-doped pentacene suggest that the correlation effects come into play distinctly between superconducting and non-superconducting systems.

In this Letter, in order to resolve the issue of correlation effects in hydrocarbon-based superconductors, we have investigated their electronic structures systematically, employing the dynamical mean-field theory (DMFT). Based on the ground state electronic structures, we have constructed the phase diagram of hydrocarbon molecular solids as functions of doping and relevant energy parameters including the Coulomb correlation, the Hund coupling, and the molecular-orbital

(MO) energy level splitting. Our studies reveal that hydrocarbon-based superconductors belong to multi-band Fermi liquid system, while non-superconducting K-doped pentacene belongs to single-band system in the proximity of the MIT. Further, we have shown that the energy level splitting between LUMO+1 and LUMO (lowest unoccupied MO) plays a key role in the superconductivity of electron-doped hydrocarbon molecular solids.

Both picene and pentacene solids have layered crystal structures, as shown in Fig. 1(a). Picene molecule has an arm-chair type structure (Fig. 1(b)), while pentacene molecule has a linear arrangement of benzene rings (Fig. 1(c)). The difference in molecular structures produces the different electronic structures in three electron-doped picene (picene³⁻) and pentacene (pentacene³⁻). As shown in Fig. 1(d) and (e), the energy level splitting Δ between LUMO+1 and LUMO of picene solid

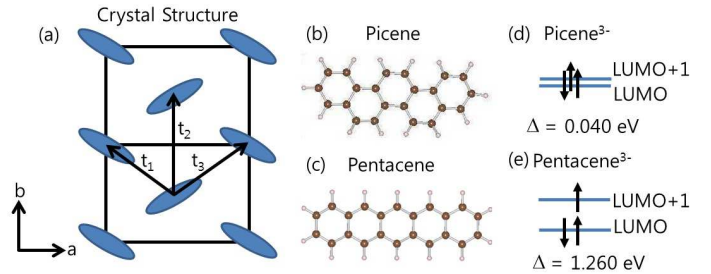


FIG. 1: (Color online) (a) Crystal structure of picene and pentacene solids. Blue ellipses represent picene or pentacene molecular units shown in (b) and (c). t_1 , t_2 , t_3 are hopping amplitudes along each direction. (b) Molecular structure of picene. (c) Molecular structure of pentacene. (d) MO energy levels and occupation of electrons for picene³⁻ solid. (e) The same for pentacene³⁻ solid. Note that the energy level splitting (Δ) between LUMO+1 and LUMO for picene solid ($\Delta = 0.040$ eV) is much smaller than that of pentacene solid ($\Delta = 1.260$ eV).

TABLE I: Hopping amplitudes $t_{l,m,\mathbf{R}}$ (in meV) determined from the *ab initio* band structures of picene and pentacene solids, where l and m represent the MOs, and \mathbf{R} represents the hopping direction in the lattice. Subscript 1,2,3 represent the hopping directions as shown in Fig 1, and c represents the direction normal to *ab* plane.

	$t_{L+1,L,0}$	$t_{L+1,L+1,1}$	$t_{L,L,1}$	$t_{L+1,L+1,2}$	$t_{L,L,2}$	$t_{L+1,L+1,3}$	$t_{L,L,3}$	$t_{L+1,L+1,c}$	$t_{L,L,c}$	$t_{L+1,L,c}$
Picene	-10	40	-40	-30	-50	-20	-20	0	0	20
Pentacene	0	60	70	-10	-30	-30	-60	-10	-10	0

($\Delta = 0.04$ eV) is much smaller than that of pentacene solid ($\Delta=1.26$ eV). Because the bandwidth of each orbital in both molecular solids is ~ 0.25 eV, picene³⁻ has the occupation of three electrons on nearly two-fold degenerate orbitals,[11, 13, 16] whereas pentacene³⁻ has one electron on the single LUMO+1 orbital that is far separated from the lower LUMO.

The correlation effects in electron-doped hydrocarbon solids are dealt with by the following two-band Hubbard model Hamiltonian,

$$\begin{aligned}
 H &= H_0 + H_I, \\
 &= \sum_{l,m,\mathbf{R},\sigma} t_{l,m,\mathbf{R}} c_{l,\mathbf{R},\sigma}^\dagger c_{m,0,\sigma} + H_I, \quad (1)
 \end{aligned}$$

where H_0 and H_I are non-interacting and interacting Hamiltonians of doped electrons, respectively. Here $t_{l,m,\mathbf{R}}$ corresponds to hopping from $(0,m)$ to (\mathbf{R},l) , where 0 and \mathbf{R} represent sites, m and l represent the MOs. We have determined $t_{l,m,\mathbf{R}}$, using the downfolding scheme of Kohn-Sham orbitals in the maximally localized Wannier function (MLWF) basis.[17–19] Kohn-Sham orbitals were obtained in the generalized gradient approximation (GGA), by employing the full-potential augmented plane wave (FLAPW) band method[20] implemented in WIEN2k package.[21] For electron-doped systems, we have utilized the rigid band approximation due to the absence of experimental crystal structures. We have employed experimental crystal structures for undoped picene and pentacene.[22, 23] We have confirmed that the structure optimization in the GGA does not change the original undoped crystal structures much. The obtained hopping parameters $t_{l,m,\mathbf{R}}$ are provided in Table I.

H_I is given approximately by

$$\begin{aligned}
 H_I &= U \sum_{m,\mathbf{R}} n_{m,\mathbf{R},\uparrow} n_{m,\mathbf{R},\downarrow} + U' \sum_{m>l,\mathbf{R},\sigma} n_{m,\mathbf{R},\sigma} n_{l,\mathbf{R},\sigma} \\
 &+ (U' - J) \sum_{m>l,\mathbf{R},\sigma} n_{m,\mathbf{R},\sigma} n_{l,\mathbf{R},\sigma}, \quad (2)
 \end{aligned}$$

where U , U' and J are intra-, inter-orbital Coulomb correlation and Hund interaction parameters, respectively. We considered here rotationally symmetric interaction, so that $U_{LUMO+1} \sim U_{LUMO}$ and $U' \sim U - 2J$. [13] We have solved the above Hamiltonian by carrying out the DMFT calculation.[24] We used the continuous time quantum Monte-Carlo (CTQMC) method as an impurity solver.[25, 26] We set temperature at $T=77$ K ($=6.67$

meV), which is low enough to observe the MIT in the phase diagram of hydrocarbon solids.[27]

Figure 2 shows the imaginary part of the obtained Green's function $G(i\omega_n)$ and the self-energy $\Sigma(i\omega_n)$ for LUMO+1 and LUMO of picene³⁻ solid. For $U = 0.45$ eV, $\text{Im}G(i\omega_n)$'s of both LUMO+1 and LUMO have finite values at $\omega_n = 0$ (ω_n : Matsubara frequency), implying that the densities of states (DOSs) at the Fermi level (E_F) are finite for both orbitals. Also $\text{Im}\Sigma(i\omega_n)$'s for both MOs converge to zero in the zero frequency regime, signifying the Fermi liquid nature. Note that the magnitude of $\text{Im}\Sigma(i\omega_n)$ is significantly larger for LUMO+1 than for LUMO, which reflects that the electronic correlation is stronger for LUMO+1. In fact, $U = 0.45$ eV corresponds to the value obtained from the first-principles calculation for picene³⁻ solid.[13] So these results indicate that K₃picene solid in its normal state has two-band Fermi liquid nature with clear orbital-selective band renormalization.

For $U=0.65$ eV, $\text{Im}G(i\omega_n)$'s near $\omega_n = 0$ appear to be finite for both LUMO+1 and LUMO, but that for LUMO has negative slope. From the derivative of $\text{Im}G(i\omega_n)$ near $\omega_n = 0$ one can distinguish between metallic and insu-

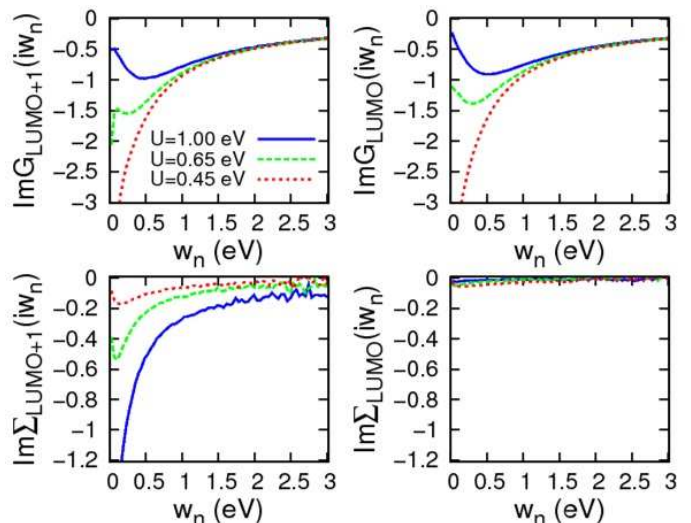


FIG. 2: (Color online) Imaginary Green's functions $G(i\omega_n)$ and self energies $\Sigma(i\omega_n)$ of LUMO+1 and LUMO for picene³⁻ solid ($J=0.05$ eV and $\Delta=0.04$ eV). Red (dotted), green (dashed), and blue (solid) lines are for $U=0.45$ eV, $U=0.65$ eV, and $U=1.00$ eV, respectively.

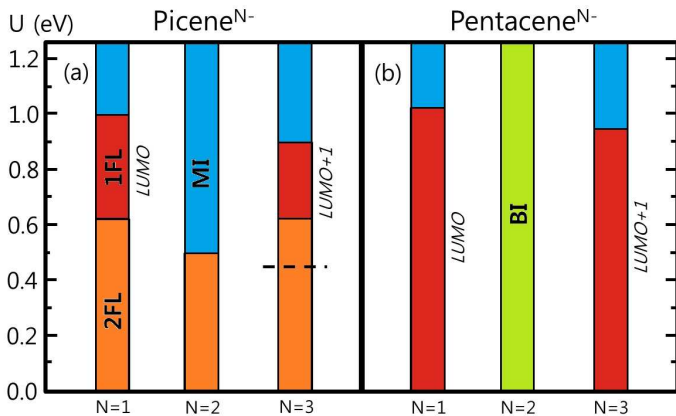


FIG. 3: (Color online) (a) Ground states of picene solid ($J=0.05$ eV and $\Delta=0.04$ eV) with variations of doping ($N=1, 2$, and 3) and Coulomb interaction (U). (b) Ground states of pentacene solid ($J=0.05$ eV and $\Delta=1.26$ eV). 1FL, 2FL, BI, and MI stand for one-band Fermi liquid, two-band Fermi liquid, band insulator, and Mott insulator, respectively. Dashed line for picene³⁻ corresponds to the U value obtained from the first-principles calculation.[13]

lating phases as shown in previous literatures.[28, 29]. We consider that positive (negative) derivative illustrates the metallic (insulating) electronic structure. Accordingly, only the LUMO+1 band has nonzero DOS at E_F . The behaviors of $\text{Im}G(i\omega_n)$ and $\text{Im}\Sigma(i\omega_n)$ of LUMO+1 for $U=0.65$ eV reflect that the system belongs to narrow single-band Fermi liquid state. For $U=1.0$ eV, both $\text{Im}G(i\omega_n)$'s are vanishing at $\omega_n = 0$, implying that DOSs at E_F are zero for both LUMO+1 and LUMO. $\text{Im}\Sigma(i\omega_n)$ at $\omega_n = 0$ diverges for LUMO+1, indicating that the system has the Mott insulating state with hole-orbital disproportionation nature at LUMO+1. Namely, the hole orbital nature changes from the mixture of LUMO and LUMO+1 to the single LUMO+1 (see the inset of Fig. 5).

Figure 3 shows the ground states of picene and pentacene solids depending on doping N and the U value. We have obtained the ground states by following the steps in Fig. 2. As mentioned above, picene³⁻ solid, which has $U = 0.45$ eV, belongs to the two-band Fermi liquid state.[30] This feature reveals that the superconductivity in three electron-doped picene, such as K₃picene and Ca_{1.5}picene, emerges from the multi-band Fermi liquid state. If we increase U further for picene³⁻, single-band (LUMO+1) Fermi liquid state is realized at $U=0.625$ eV, and the Mott insulating state at $U=0.90$ eV. In the DMFT calculation, Ruff *et al.*[14] used $U=1.6$ eV, which was estimated from the empirical cavity method for the screening of electronic correlation.[12] This U value is considerably larger than $U = 0.45$ eV obtained from the first-principles calculation.[13, 30] That is why Ruff *et al.* obtained the Mott insulating state for K₃picene in contrast to our result. Nevertheless, the occurrence of the MIT for large U is consistent between

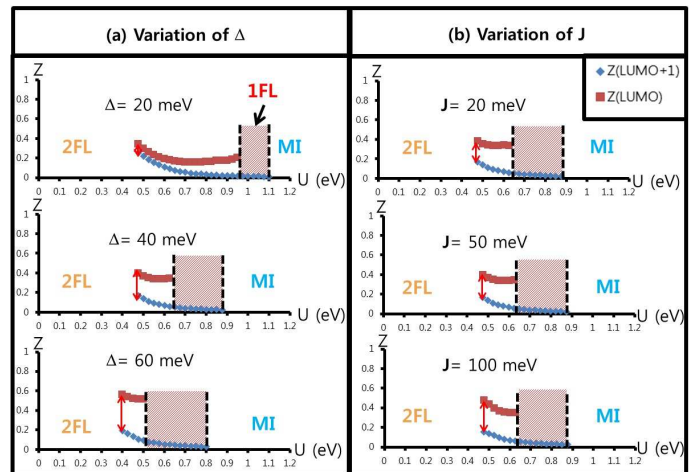


FIG. 4: (Color online) (a) Quasi-particle residue Z 's of LUMO+1 and LUMO vs. U for picene³⁻ solid with variation of Δ ($J=50$ meV). (b) The same for picene³⁻ solid with variation of J ($\Delta=40$ meV). Red arrow denotes the difference of Z 's between LUMO+1 and LUMO.

two.

Similarly to picene³⁻, picene¹⁻ solid also shows the phase transition upon increasing U , from two-band to one-band (LUMO) Fermi liquid state, and then to the Mott insulating state. In the case of picene²⁻, due to the finite Hund coupling J ($=0.05$ eV), the system for small U remains as two-band Fermi liquid state with high-spin configuration. With increasing U , the phase transition occurs directly from two-band Fermi liquid to Mott insulating state. If one takes into account the non-rigidity of band structures arising from the hybridization with cations in K- or Ca-doped picene, the electronic correlation effect would be further reduced with respect to the above rigid band case.[19] Then K₃picene and Ca_{1.5}picene would have more stable two-band Fermi liquid nature in their normal states. If the K doping level is biased from the integer value, the correlation effect would be not so significant as for the integer doping case. As a result, one would obtain the stable two-band Fermi liquid state for the non-integer doping case too. However, in the case of non-integer doping, the disorder effect is expected to become important. In fact, the insulating nature in superconducting K_xpicene ($x = 3.1, 3.5$) observed above T_C was explained by the granular-metal-like behavior, which would be attributed to the disorder effect.[31]

Noteworthy in Fig. 3(b) is that the ground state of pentacene³⁻ is very different from that of picene³⁻. Due to much larger Δ value in pentacene, both pentacene³⁻ and pentacene¹⁻ solids exhibit the transition from single-band Fermi liquid to Mott insulator, like a single-band half-filled system. On the other hand, pentacene²⁻ has the low-spin state due to large Δ , and so only the band insulating state is realized. The findings in Fig. 3 mani-

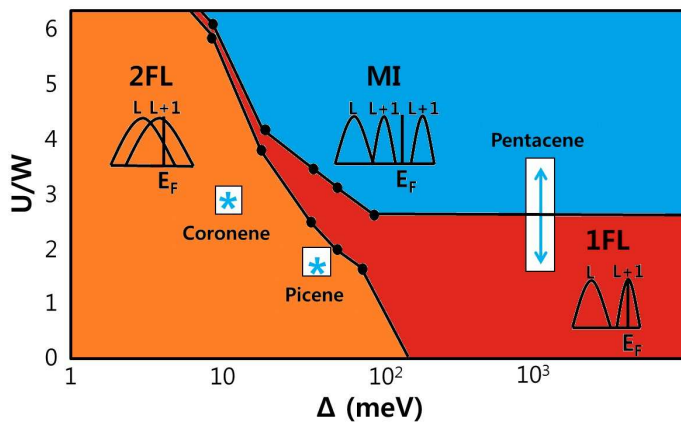


FIG. 5: (Color online) Phase diagram of hydrocarbon³⁻ solids with respect to Coulomb correlation U and MO level splitting Δ . Positions of picene³⁻, coronene³⁻, and pentacene³⁻ solids are marked in the phase diagram. Inset diagram represents the schematic DOS of each phase. In the MI regime, the hole-orbital disproportionation nature is realized.

fest that different Δ 's of picene and pentacene play key roles in producing the different phases. Also high-spin and low-spin configurations of picene²⁻ and pentacene²⁻ suggest that the Hund coupling J affects the phase diagram.

Figure 4 presents the quasi-particle residue Z for picene³⁻ solid with the variation of Δ and J . The quasi-particle residue Z is obtained from $Z = (1 - \frac{Im\Sigma(iw_0)}{w_0})^{-1}$, where w_0 is the lowest Matsubara frequency.[28] With increasing Δ , the following features are observed in Fig. 4(a): (i) the larger difference of Z 's between LUMO+1 and LUMO, (ii) the wider single-band (LUMO+1) Fermi liquid regime, and (iii) the reduced critical U for the MIT. The above observations indicate that just a small enhancement of Δ would induce the single-band Fermi liquid state in picene³⁻ solid, and thereby suppress the superconductivity. This sensitive dependence of electronic structure of picene³⁻ upon variation of Δ explains different experimental electronic structures of K₃picene solid depending on the preparation condition.[14, 31–33] As shown in Fig. 4(b), the larger J also yields the larger difference of Z 's between LUMO+1 and LUMO. But the single-band Fermi liquid regime and the critical U value for the MIT do not change much. Larger difference of Z 's between two MOs implies that the inter-orbital fluctuation becomes suppressed. Therefore Fig. 4 indicates that the larger Δ induces the orbital disproportionation, and the larger J suppresses the inter-orbital fluctuation.[34]

Figure 5 presents the overall phase diagram of hydrocarbon³⁻ solids as functions of U and Δ . The ground state of picene³⁻ solid is two-band Fermi liquid state. In contrast, the ground state of pentacene³⁻ solid is single-band Fermi liquid or Mott insulator de-

pending on U value.[35] This difference is the reason why picene³⁻ is superconducting, while pentacene³⁻ is non-superconducting. The ground states of K₃coronene and K₃phenanthrene in their normal states are also two-band Fermi liquid states, with three doped electrons occupying nearly degenerate LUMO and LUMO+1. On the other hand, 1,2;8,9-dibenzopentacene has large energy splitting between LUMO and LUMO+1, but nearly degenerate LUMO+1 and LUMO+2.[36] Hence K₃1,2;8,9-dibenzopentacene has one electron on the nearly degenerate LUMO+1 and LUMO+2. This situation is similar to that of picene¹⁻ in Fig. 3(a).

Dopant-induced structural deformation and hybridization are to be reflected in the variation of Δ and U/W in Fig.5. For example, the total bandwidth of K₃picene is enhanced with respect to that of undoped picene, from ~ 0.35 eV to ~ 0.60 eV.[19] As a result, the position of K₃picene would be further lowered than that of picene³⁻ in the phase diagram of Fig. 5.[37] Therefore the phase diagram of Fig. 5 demonstrates that the superconductivity in hydrocarbon-based superconductors commonly emerge from the two-band Fermi liquid state with good metallic nature. This feature supports the conventional phonon-mediated BCS mechanism rather than other exotic mechanisms for the superconductivity of hydrocarbon-based molecular solids,[38–41] despite that they have U/W larger than one. The underlying superconducting mechanism in hydrocarbon-based superconductors needs further investigation, but it is evident that the superconductivity would be boosted up by the enhanced DOS at E_F due to their two-band Fermi liquid nature.[38] Our phase diagram indicates that small U/W and Δ are key factors for the emergence of superconductivity in hydrocarbon-based molecular solids. Thus the superconductivity is preferentially to be searched for in closely packed hydrocarbon-based molecular solids that have small U/W and Δ .

In conclusion, we have investigated the electronic structures of electron-doped hydrocarbon solids based on the DMFT calculations, and constructed the phase diagram with respect to Coulomb correlation U , doped electrons N , Hund coupling J , and MO energy level splitting Δ . We have shown that the superconductivity in hydrocarbon solids commonly emerges from the two-band Fermi liquid state. This is in contrast to the case of non-superconducting pentacene, which has the effective single-band Fermi liquid state in the proximity of the MIT. The size of MO energy level splitting plays an important role in determining the ground states of hydrocarbon solids. Our results demonstrate that multi-band nature in hydrocarbon solids is essential to boost the superconductivity through the enhanced DOS at E_F . It is thus suggested that higher T_C superconductors need to be searched for in more closely packed molecular solids with multi-band nature at E_F .

Discussions with Ki-Seok Kim and Beom Hyun Kim

are gratefully acknowledged. This work was supported by the National Research Foundation of Korea (Grant Nos. 2009-0079947, 2010-0006484, R32-2008-000-10180-0).

* E-mail: jhshim@postech.ac.kr

† E-mail: bimin@postech.ac.kr

- [1] R. Bauer, A. Schmid, P. Pavone, and D. Strauch, *Phys. Rev. B* **57**, 11276 (1998).
- [2] H. J. Choi, D. Roundy, H. Sun, M. L. Cohen, and S. G. Louie, *Nature* **418**, 758 (2002).
- [3] P. A. Lee, N. Nagaosa, and X. -G. Wen, *Rev. Mod. Phys.* **78**, 17 (2006).
- [4] K. Haule, J. H. Shim, and G. Kotliar, *Phys. Rev. Lett.* **100**, 226402 (2008).
- [5] G. Csányi, P. B. Littlewood, A. H. Nevidomskyy, C. J. Pickard, and B. D. Simons, *Nature Phys.* **1**, 42 (2005).
- [6] M. Capone, M. Fabrizio, C. Castellani, and E. Tosatti, *Rev. Mod. Phys.* **81**, 943 (2009).
- [7] R. Mitsuhashi, Y. Suzuki, Y. Yamanari, H. Mitamura, T. Kambe, N. Ikeda, H. Okamoto, A. Fujiwara, M. Yamaji, N. Kawasaki, Y. Maniwa, and Y. Kubozono, *Nature* **464**, 76 (2010).
- [8] Y. Kubozono, H. Mitamura, X. Lee, X. He, Y. Yamanari, Y. Takahashi, Y. Suzuki, Y. Kaji, R. Ehuchi, K. Akaike, T. Kambe, H. Okamoto, A. Fujiwara, T. Kato, T. Kosugi, and H. Aoki, *Phys. Chem. Chem. Phys.*, **13**, 16476 (2011).
- [9] X. F. Wang, R. H. Liu, Z. Gui, Y. L. Xie, Y. J. Yan, J. J. Ying, X. G. Luo, and X. H. Chen, *Nature Comm.* **2**, 507 (2011).
- [10] M. Xue, T. Cao, D. Wang, Y. Wu, H. Yang, X. Dong, J. He, F. Li and G. F. Chen, *Sci. Rep.* **2**, 389 (2012).
- [11] M. Kim, B. I. Min, G. Lee, H. J. Kwon, Y. M. Rhee, and J. H. Shim, *Phys. Rev. B* **83**, 214510 (2011).
- [12] G. Giovannetti and M. Capone, *Phys. Rev. B* **83**, 134508 (2011).
- [13] Y. Nomura, K. Nakamura, and R. Arita, *Phys. Rev. B* **85**, 155452 (2012).
- [14] A. Ruff, M. Sing, R. Claessen, H. Lee, M. Tomić, H. O. Jeschke, and R. Valentí, *Phys. Rev. Lett.* **110**, 216403 (2013).
- [15] M. F. Craciun, G. Giovannetti, S. Rogge, G Brocks, A. F. Morpurgo, and J. van den Brink, *Phys. Rev. B* **79**, 125116 (2009).
- [16] T. Kosugi, T. Miyake, S. Ishibashi, R. Arita, and H. Aoki, *J. Phys. Soc. Jpn.* **78**, 113704 (2009).
- [17] A. A. Mostofi, J. R. Yates, Y. -S. Lee, I Souza, D. Vanderbilt, and N. Marzari, *Comp. Phys. Comm.* **178**, 685 (2008).
- [18] MLWF provides lower and upper Wannier functions, which are $\frac{1}{\sqrt{2}}(\psi_{LUMO+1} + \psi_{LUMO})$ and $\frac{1}{\sqrt{2}}(\psi_{LUMO+1} - \psi_{LUMO})$. [16, 19] We applied the unitary transform to obtain Hamiltonian H_0 with LUMO+1 and LUMO basis.
- [19] T. Kosugi, T. Miyake, S. Ishibashi, R. Arita, and H. Aoki, *Phys. Rev. B* **84**, 214506 (2011).
- [20] M. Weinert, E. Wimmer, and A. J. Freeman, *Phys. Rev. B* **26**, 4571(1982).
- [21] P. Blaha, K. Schwarz, G.K.H. Madsen, D. Kvasnicka, J. Luitz, WIEN2k (Karlheinz Schwarz, Technische Universität Wien, Austria, 2001).
- [22] A. De, R. Ghosh, S. Roychowdhury, and P. Roychowdhury, *Acta Cryst.* **C41**, 907 (1985).
- [23] R. B. Campbell, J. M. Robertson, and J. Trotter, *Acta Cryst.* **14**, 705 (1961).
- [24] G. Kotliar, S. Y. Savrasov, K. Haule, V. S. Oudovenko, O. Parcollet, and C. A. Marianetti, *Rev. Mod. Phys.* **78**, 865 (2006).
- [25] K. Haule, *Phys. Rev. B* **75**, 155113 (2007).
- [26] P. Werner, A. Comanac, L. de' Medici, M. Troyer, and A. J. Millis, *Phys. Rev. Lett.* **97**, 076405 (2006).
- [27] A. Georges, G. Kotliar, W. Krauth, and M. J. Rozenberg, *Rev. Mod. Phys.* **68**, 13 (1996).
- [28] R. Kováčik, P. Werner, K. Dymkowski, and C. Ederer, *Phys. Rev. B* **86**, 075130 (2012).
- [29] S. Fuchs, E. Gull, M. Troyer, M. Jarrell, and T. Pruschke, *Phys. Rev. B* **83**, 235113 (2011).
- [30] Here U is corresponding to an effective Coulomb interaction that is given by $\bar{U}-\bar{V}$ in Ref.[13], where \bar{U} and \bar{V} represent on-site and nearest neighboring Coulomb interactions, respectively.
- [31] K. Teranishi, X. He, Y. Sakai, M. Izumi, H. Goto, R. Eguchi, Y. Takabayashi, T. Kambe, and Y. Kubozono, *Phys. Rev. B* **87**, 060505(R) (2013).
- [32] B. Mahns, F. Roth, and F. Knupfer *J. Chem. Phys.* **136**, 134503 (2012).
- [33] M. Caputo, G. D. Santo, P. Parisse, L. Petaccia, L. Floreano, A. Verdini, M. Panighel, C. Struzzi, B. Taleatu, C. Lal, and A. Goldoni, *J. Phys. Chem. C* **116**, 19902 (2012).
- [34] L. de' Medici, *Phys. Rev. B* **83**, 205112 (2011).
- [35] First-principle result of U for pentacene³⁻ is not available. The range of U in Fig. 5 corresponds to that in-between the first-principles (Ref.[13]) and the empirically calculated U (Ref.[11]) for picene³⁻.
- [36] B. Mahns, F. Roth, A. König, M. Grobosch, M. Knupfer, and T. Hahn, *Phys. Rev. B* **86**, 035209 (2012).
- [37] There are several metastable structures for K₃picene.[14, 19, 31–33] Determination of Δ and U/W for each metastable structure would be an interesting future problem.
- [38] T. Kato, T. Kambe, and Y. Kubozono, *Phys. Rev. Lett.* **107**, 077001 (2011).
- [39] M. Casula, M. Calandra, G. Profeta, and F. Mauri, *Phys. Rev. Lett.* **107**, 137006 (2011).
- [40] M. Casula, M. Calandra, and F. Mauri, *Phys. Rev. B* **86**, 075445 (2012).
- [41] A. Subedi, and L. Boeri, *Phys. Rev. B* **84**, 020508(R) (2011).